A New Combination of Conditional Environmental Distributions

Jan-Tore Horn[a,b,*], Elzbieta Bitner-Gregersen[c], Jørgen R. Krokstad[b], Bernt J. Leira[b], Jørgen Amdahl[a,b]

[a] *Centre for Autonomous Marine Operations and systems (NTNU AMOS), NTNU, Trondheim, Norway*
[b] *Department of Marine Technology, NTNU, Trondheim, Norway*
[c] *DNV GL, Veritasveien 1, Høvik, Norway*

Abstract

In this paper, a joint distribution of all relevant environmental parameters used in design of offshore structures including directional components is presented, along with a novel procedure for dependency modelling between wind and wind sea. Probabilistic directional models are rarely used for response calculation and reliability assessments of stationary offshore structures. However, very few locations have the same environment from all compass directions in combination with a rotationally symmetric structure. The scope of this work is to present a general environmental joint distribution with directional descriptions for long term design of stationary offshore structures such as offshore wind turbines. Wind, wind sea and swell parameters will be investigated for a chosen location in the central North Sea.

Keywords: joint distribution; environmental parameters; directional effects; design; offshore wind turbines

1. Introduction

The present work presents a general multi-dimensional joint distribution which is fitted to data from the site of a future offshore wind farm in the central North Sea. The aim is to obtain a statistical representation of combinations of all relevant environmental variables for design of offshore wind turbines where absolute and relative load directions are important for response analyses. The proposed model is useful for full long term analyses to calibrate simplified design methods, and finding probable combinations of environmental parameters for extreme sea states and simplified ULS design [1]. Environmental variables include wind, wind sea, swell and tide, as well as their respective directions.

*Corresponding author
Email address: jan-tore.horn@ntnu.no (Jan-Tore Horn)

A conditional modelling approach [2] will be utilized, due to its robustness for description of simultaneous information in data. Copula-based methods may be an alternative, but still need further exploration [3, 4, 5].

Depending on the desired accuracy of the structural response and reliability estimations, the joint environmental distributions can be extended to high dimensions corresponding to the available site-specific data. Accounting for environmental variable correlations has shown to reduce design conservatism [6] for structures related to oil and gas extraction on the Norwegian continental shelf. Joint modelling of offshore environmental processes has evolved over the years to facilitate probabilistic analysis of structures. Early adoptions include a bottom-fixed structure accounting for wave height and current [7]. A comprehensive omni-directional model including wind, wave, current and tidal elevation can be found in e.g. [8], and it is often referred to by standards for joint modelling of environmental processes [9]. A similar model is used in e.g. [10], adopted for the northern North Sea and more recently in [11] for several locations. In [12], an extension is added to model the mean and standard deviation of the wind and wave direction. Later, a model for description of combined sea (wind sea and swell) and relative directions was presented in e.g. [13]. It is still a challenge to model directional processes. For instance, consistency with regard to combining omni-directional and multi-directional data must be considered in probabilistic design [14].

For offshore wind turbines, the structural dynamics with a power-producing rotor will introduce directionally dependent response characteristics [15, 16, 17]. Hence, a statistical description of both absolute and relative directions of the load processes is of importance. A continuous wave directional distribution can be found in e.g. [18] and combined with a structural resistance in [19] as a function of the absolute direction. Further, a model for relative wind-wave direction was proposed in [20], but lacks relation to the earth-fixed coordinate system, which will be introduced in the present work.

In [21] and [22], the absolute wind direction was modelled using the von Mises distribution [23, 24], which has proven suitable for circular distributions. Furthermore, a relation between wind speed and direction was presented in [25]. This dependency will be also explored in this paper, with a slightly more pragmatic approach and in combination with other relevant offshore environmental processes.

The present study proposes a new combination of conditional environmental distributions which can be found in the literature and verifies it by environmental data from the North Sea. The paper is organized as follows: First, the example offshore site is presented along with the data characteristics before and after pre-processing. Secondly, the full environmental join distribution is constructed along with evaluation of the goodness of the conditional fittings. Finally, an error test of the complete distribution is performed.

2. Offshore site

Hindcast data for description of the wind and wave environment used in the study is provided by the Norwegian Meteorological Institute [26] for the location shown in Fig. 1. The data contains information about the wind speed, wind direction and significant wave height, peak period, and direction for both wind sea and swell. The data are sampled every third hour and cover the historical period of approximately 60 years.

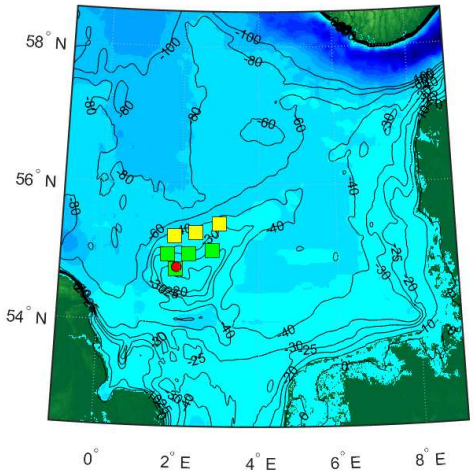

Figure 1: Planned (green) and possible (yellow) offshore wind farms at Dogger Bank with location for hindcast data (red)

The hindcast data are pre-processed in order to remove ties due to discrete frequencies in the hindcast model, and to make the data independent and identically distributed (iid). This is done by de-seasonalizing the raw data with a moving average algorithm. De-seasoning is one of the suggested pre-processing methods when using data from measurements [27]. Note that directional data is not pre-processed. The effects of pre-processing can be seen in Fig. 2 and 3. It is clear that the de-seasonalizing algorithm reduces the tail-distribution of the wind speed and significant wave height, yielding smaller extreme values. The average conditional exceedance rate (ACER) approach as described in [28] is plotted in Fig. 3 for two values of the conditioning parameter k. In the ACER method, k consecutive peaks over a given exceedance level will be considered dependent and only the first peak will be counted. It is seen that de-seasonalizing has a large effect on the high-percentile values, but the ACER method varies from the wind speed to the wave height, indicating a higher inter-dependency in the wave height hindcast data. This is reflected in Tab. 1 where the ACER method has a much larger impact on the extreme values for wave height.

	V [m/s]		H_S^w [m]	
k	1	2	1	2
Raw	32.74	32.61	9.07	8.68
De-seasoned	30.35	29.96	8.62	7.94

Table 1: 50-year values using the ACER method with and without de-seasonalizing

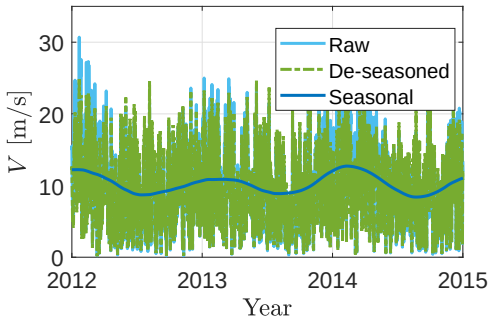

(a) Wind speed

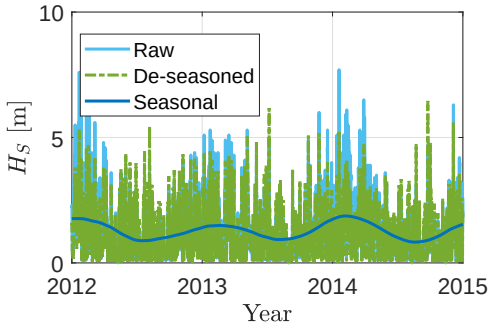

(b) Wind sea significant wave height

Figure 2: De-seasonalizing of wind and wind sea

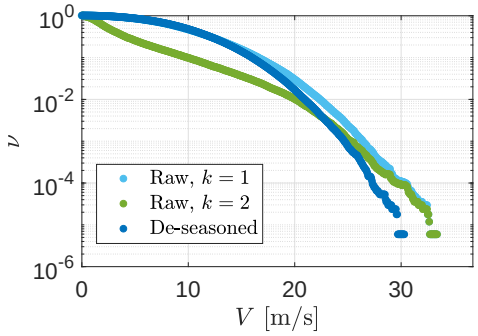

(a) Wind speed

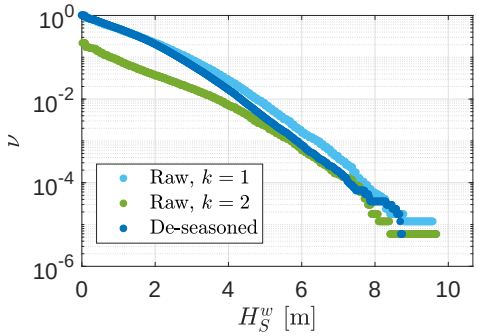

(b) Wind sea significant wave height

Figure 3: Upcrossing rates by ACER method and de-seasonalizing

Scatters of the data before and after pre-processing are shown in Fig. 4 for wind speed, significant wave height and peak period for wind sea. The pre-processed data appears to be more densely distributed, and the ties created by binning of the peak period are removed solely by de-seasonalizing.

3. Environmental joint distribution

Before constructing the environmental joint distribution, some observations and assumptions are made regarding the measurement data. First, the wind sea and swell components of the wave environment are assumed to be uncorrelated and treated separately. This has no effect on extreme wave heights or the distribution tail, but the average wind sea significant wave height is smaller than the expected total sea significant wave height. Thus, the separation is expected to reduce conservatism related to fatigue, but retains the extreme wave loads. Due to the sheltering effect of the British Islands, the wave climate in the central North Sea is mostly dominated by wind sea [29], and the swell is mainly propagating in a southerly direction [17]. Second, the astronomical

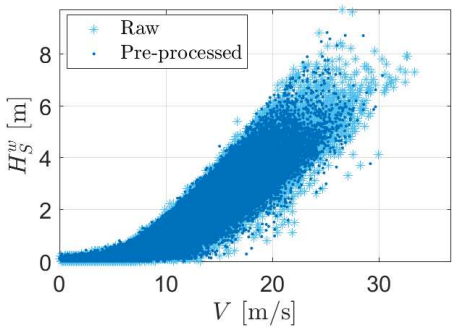

(a)

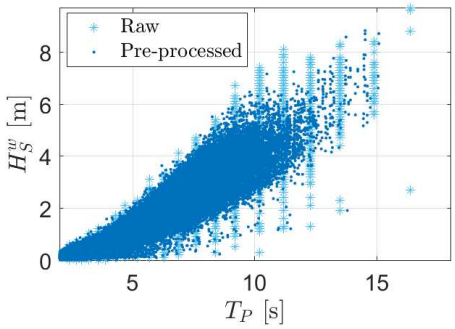

(b)

Figure 4: Hindcast data before and after pre-processing using a de-seasoning algorithm

tide is assumed uncorrelated with both the wind sea and swell. It should be noted that the design standards require the storm surge component of the water level and wind generated current to be accounted for. However, these effects are not considered in the present work, but would otherwise be included as wind sea dependent parameters. As a result, the complete joint distribution can be written as:

$$f_{\mathbf{X}_e} = f_{\mathbf{X}_w} \cdot f_{\mathbf{X}_s} \cdot f_{H_t} \tag{1}$$

where the wind sea and swell parameters are gathered in:

$$\begin{aligned} \mathbf{X}_w &= [V, \Theta_v, H_S^w, T_P^w, \Theta_w^r] \\ \mathbf{X}_s &= [H_S^s, T_P^s, \Theta_s] \end{aligned} \tag{2}$$

respectively, and described in Tab. 2 with distribution types used for marginal and conditional formulations. Note that the wind speed and direction are obtained from hindcast data at 100 meter above sea level (m.a.s.l.) for compatibility with future offshore wind farms, and to reduce the uncertainty that arises

from manual extrapolation of the wind speed at 10 m.a.s.l. An average power-law exponent for wind speed extrapolation from 10 to 100 m.a.s.l. of 0.07 (18% increase) and a standard deviation of 0.05 is observed in the hindcast data. This uncertainty is removed when using the 100 m.a.s.l. values directly. The dependencies between the environmental parameters are modelled using conditional fitting parameters, which is the industry standard [9]. Other approaches have been investigated, such as copula-based methods [4], but the traditional method with parameter fitting has proven the most robust and practical.

Table 2: Marginal distribution types and description of environmental parameters

	Parameter		Distribution	Description	Unit
Wind sea	V	v	3-p Weibull	Wind speed at 100 m.a.s.l.	[m/s]
	Θ_v	θ_v	von Mises mix	Wind direction at 100 m.a.s.l.	[deg]
	H_S^w	h_w	3-p Weibull	Significant wave height for wind sea	[m]
	T_P^w	t_w	Lognormal	Peak period for wind sea spectrum	[m]
	Θ_w^r	θ_w	Trunc. Normal	Relative wind-wave direction	[deg]
Swell	H_S^s	h_s	3-p Weibull	Significant wave height for swell	[m]
	T_P^s	t_s	Lognormal	Peak period for swell spectrum	[s]
	Θ_s	θ_s	von Mises mix	Swell direction	[deg]
	H_t	H	Normal mix	Water level	[m]

The parameter dependencies can be revealed by investigating bi-variate histograms of the raw data and the correlation coefficients. For simplicity, each parameter can only depend on one other parameter, but multi-dimensional dependencies are still captured in an indirect manner. In Tab. 3, an overview is given for the dependency modelling. For instance, H_S^w is depending on V, but not vice versa. The dependencies are chosen based on the physics of environmental phenomena and by trials aiming to provide the description with minimal amount of conditional parameters. For instance, the wind direction is dependent on wind speed and not the other way around as it turned out easier to make a bounded variable conditioned on an unbounded one. More discussions on dependency modelling can be found in e.g. [20].

Table 3: Dependency table with dependent variable in rows and independent in columns

	V	Θ_v	H_S^w	T_P^w	Θ_r^w	H_S^s	T_P^s	Θ_s	H_t
V	1								
Θ_v	1	1							
H_S^w	1		1						
T_P^w			1	1					
Θ_r^w			1		1				
H_S^s						1			
T_P^s						1	1		
Θ_s						1		1	
H_t									1

The distribution parameters, e.g. the mean value, standard deviation etc., in the conditional PDFs are fitted to the pre-processed hindcast data with a least-squares algorithm and a general non-linear regression line given by:

$$p(x) = p_1 + p_2 \cdot x^{p_3} + p_4 \exp[p_5(x + p_6)^{p_7}] \tag{3}$$

for a given parameter p as a function of x with the fitting constants $p_{1,\ldots,7}$. This is an extended fitting function to those presented in e.g. [9, 12]. Since there is no need to fit seven constants for each distribution parameter, the distribution parameter regression lines are constructed individually to obtain a reasonable function for extrapolation to be presented in the next subsections. Resulting fitting parameters can be found in the appendix.

3.1. Wind and wind sea

The model for wind sea parameters is assumed to only depend on the wind speed. Also, the peak period is assumed independent of the wind speed, which is often a good assumption [11, 20]. It has also been observed that the relative direction between wind and wind sea can be described with a Normal distribution. The wind sea joint distribution is then approximated as:

$$f_{\mathbf{X}_w} \approx f_V \cdot f_{\Theta_v|V} \cdot f_{H_S^w|V} \cdot f_{T_P^w|H_S^w} \cdot f_{\Theta_w^r|H_S^w} \tag{4}$$

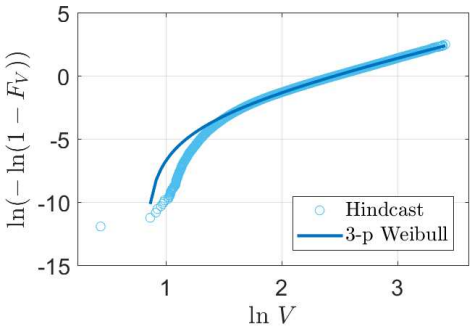

Figure 5: Wind speed data with Weibull fit

Figure 5 shows the quantile plot of the wind speed marginal distribution using the 3-parameter Weibull distribution. The wind direction is dependent on the wind speed and found to be well approximated by a combination of von Mises distributions, using the von Mises mixture distribution:

$$f_{\Theta_v|V}(\theta_v|v) = \sum_{i=1}^{n_{\theta_v}} w_i(v) \cdot f_{\Theta_v}^{(i)}(\theta_v) = \sum_{i=1}^{n_{\theta_v}} w_i(v) \frac{e^{\kappa_i \cos(\theta_v - \mu_i)}}{2\pi I_0(\kappa_i)} \tag{5}$$

where $\sum_i w_i(u) \approx 1$ and I_0 is the modified Bessel function of order zero. For the marginal distribution in Fig. 6, $n_{\theta_v} = 3$ has proven sufficient. The figure

also show the contribution from each component and both the location (μ) and the concentration parameter (κ) are kept independent of wind speed in the conditional model. The wind speed dependent weights can be found in Fig. 7, while the remaining values can be found in the appendix.

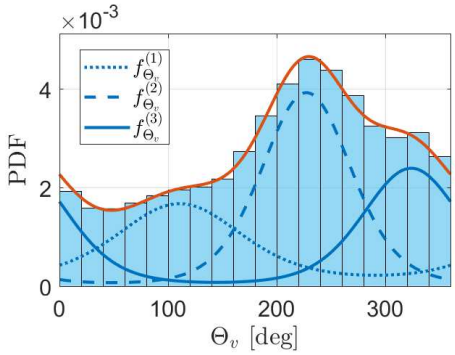

Figure 6: Marginal directional wind distribution with each von Mises component

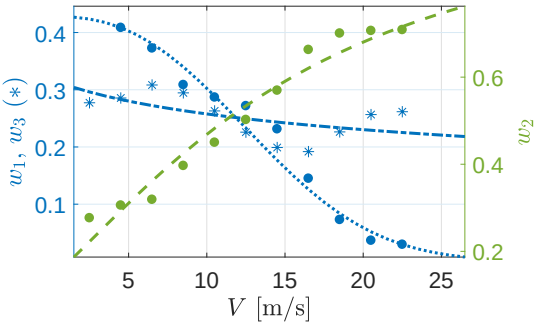

Figure 7: Fitting of weighting parameters for wind speed direction

The wind speed-conditioned directional distribution in Fig. 8 shows that strong winds are more likely to originate from the south west, which is well captured by the model.

The wind sea significant wave height conditioned on the wind speed follows a three parameter Weibull distribution as illustrated with some examples in Fig. 9a obtained with the fitted parameters in Fig. 9b. Describing the parameters in a three-parameter Weibull distribution conditionally is not presented elsewhere in the literature and may prove challenging. A good fit is observed for most H_S^w values, using a two-step fitting procedure; first, an estimation of the location parameter (γ) is performed [30] for each wind speed bin and a continuous fit is made based on Eq. 3. Second, a 2-parameter Weibull fit is performed in the same bins, correcting the data with the analytic location parameter obtained

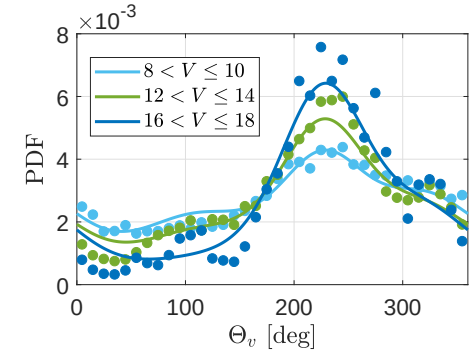

(a) PDF

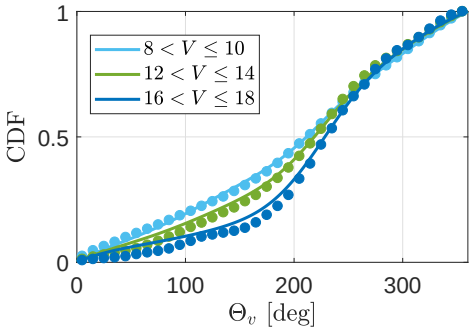

(b) CDF

Figure 8: Fitting goodness of wind direction conditioned on the wind speed

in the previous step. As a result, simple expressions are obtained as a function of the wind speed, with fitting constants given in the Appendix. Care should be taken in modelling the location parameter in order to capture the smallest values of the significant wave height, which are most probably occurring for low wind speeds as seen in Fig. 9b.

The wave peak period is dependent on the significant wave height. The fitted parameters are found in Fig. 10b and the conditional quantile plots can be found in Fig. 10a. For small wave heights, it appears that some large values of the peak period does not satisfy a Lognormal assumption. These data are probably representing swell periods, which are unsuccessfully separated from the wind sea during generation of hindcast data. Such data are also visible in Fig. 4, where some outliers in terms of small steepness are observed. Further, the wind-wave relative direction is modelled with a Normal distribution truncated on ± 90 degrees relative to the wind direction. The quantile plots in Fig. 11a shows a good fit with the parameters in Fig. 11b. Interestingly, the standard deviation is independent of the wave height, while the mean relative direction is decreasing linearly, due to a higher probability of time lag between the wind

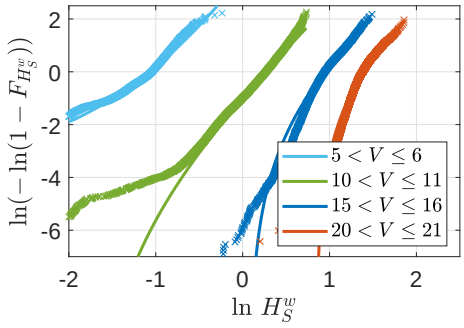

(a)

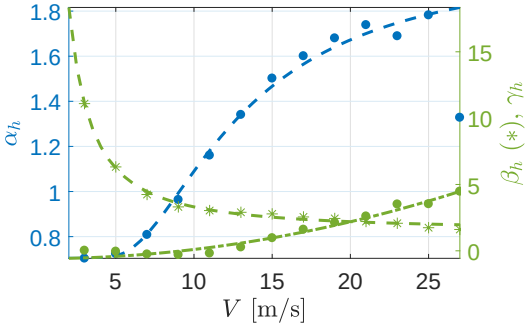

(b)

Figure 9: Wind sea significant wave height

and wave directional changes for high sea states. In other words, the relative probability of misaligned wind and wind sea is increasing with increasing wave height.

3.2. Swell

The joint distribution for swell is assumed independent of the wind sea variables and approximated as:

$$f_{\mathbf{X}_s} \approx f_{H_S^s} \cdot f_{T_P^s|H_S^s} \cdot f_{\Theta_s|H_S^s} \tag{6}$$

where the swell peak period is conditioned on the swell significant wave height and the direction of propagation is dependent on significant wave height. The 3-parameter Weibull distribution provides a good fit for the swell significant wave height as seen in Fig. 12a when $H_S^s > e^{-1} \approx 0.37$ meter. Furthermore, the swell directional distribution in Fig. 12b is approximated by a bimodal von Mises mixture distribution, representing the swell from the northern and southern North Sea. In [29], typical swell directions can be found, indicating that

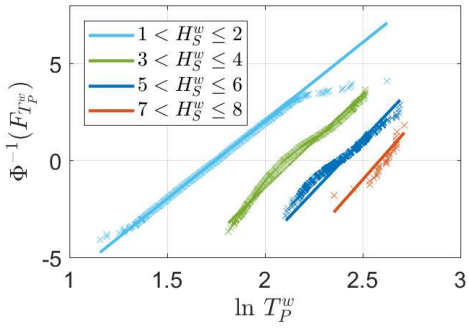

(a)

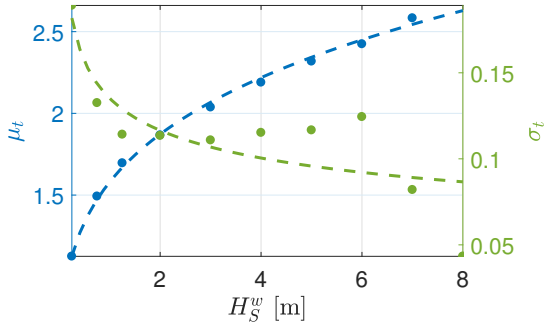

(b)

Figure 10: Wind sea peak period

swell from north originates from heavy weather in the north Atlantic sea. However, the Dogger Bank area is still dominated by wind sea due to a high degree of energy dissipation in the swell before reaching the area of interest. Swell from the south and other directions is less likely, but present in the hindcast data. Of course, the swell separation technique used by the wave spectral model by which the data were simulated might affect the predicted direction as well as the period and wave height combinations, introducing uncertainties in the data and the fitted model. It can therefore be argued that modelling the swell directional distributions may require some additional considerations, especially for the direction. The directional dependency on the swell wave height is modelled in a similar manner as the conditional wind direction, with two dominating directions:

$$f_{\Theta_s|H_S^s}(\theta_s|h_s) = \sum_{i=1}^{2} w_i(h_s) \cdot f_{\Theta_s}^{(i)}(\theta_s) = \sum_{i=1}^{2} w_i(h_s) \frac{e^{\kappa_i \cos(\theta_s - \mu_i)}}{2\pi I_0(\kappa_i)} \tag{7}$$

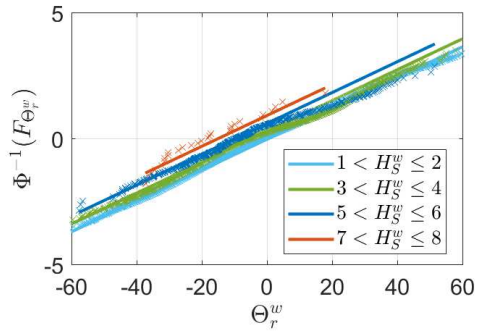

(a)

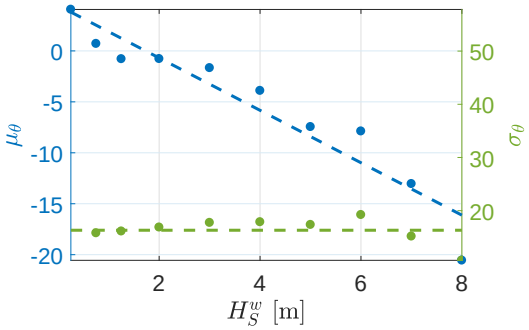

(b)

Figure 11: Wind sea relative direction

The first direction is from south, with a wide spread as seen in Fig. 12b, resulting in a close to uniform distribution. The second is from north, which is more narrow banded. With a least-squares fitting method, the best weighting parameters are found given the μ and κ parameters in the von Mises distribution obtained from the marginal fit. The result is shown in Fig. 14 with power function fits, and fitting parameters can be found in the appendix. As expected, the northern direction ($\Theta_s^{(2)}$) dominates for larger H_S^s.

The swell peak period dependence on the swell significant wave height is well captured by a conditional Lognormal distribution as seen in Fig. 13a and 13b for quantile plots and parameter fitting, respectively.

3.3. Tide

As tidal current is not expected to lead to an increased loading at the bottom-fixed wind turbines at the present site, at least in a linear manner, it is neglected in this study. However, the water level variation induced by tides may affect the wave loads significantly due to the shallow water depths and is therefore included.

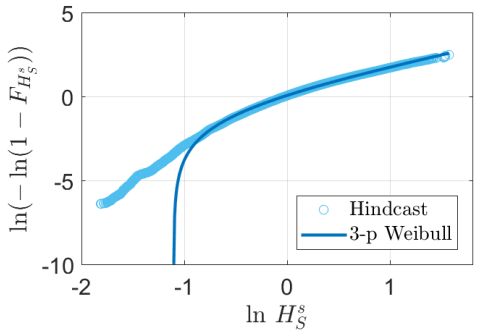

(a) Swell significant wave height

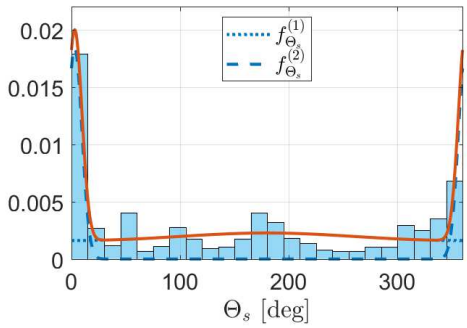

(b) Marginal swell directional distribution

Figure 12: Swell wave height and directional distribution

The tide is modelled as an independent process. By only accounting for tidal variations due to the astronomical tide, this is expected to be a good approximation. However, this may be non-conservative for three-hour analysis of extreme sea-states, as the storm duration is typically longer than three hours when including the temporal evolution. To account for the possibility of having a high sea state in combination with a high astronomical tide, the industry standards typically require extreme conditions to be modelled in combination with an high water level [27]. Other important environmental phenomena leading to currents and water level variations such as storm surge is not accounted for in the present work, but should rather be included in the description of the wind sea, wind speed dependent. The water level data is retrieved from `www.worldtide.info` for the actual location, transformed to values representative for three hour durations for compatibility with the hindcast data, and fitted to a Gaussian mixture model as illustrated in Fig. 15. Here, two components are needed for a good

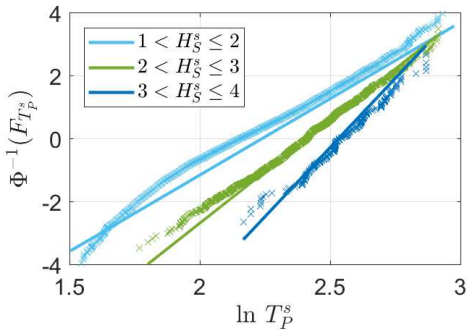

(a) Swell peak period

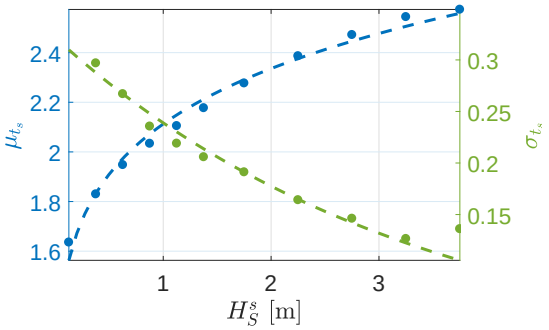

(b) Swell peak period parameters

Figure 13: Swell peak period with fitted function for the swell wave height dependent parameters

fit, and the tidal water level distribution is modelled as:

$$f_{H_t} \sim \sum_{i=1}^{2} w_i \cdot \mathcal{N}(\mu_i, \sigma_i^2) \tag{8}$$

with the fitting parameters given in the appendix.

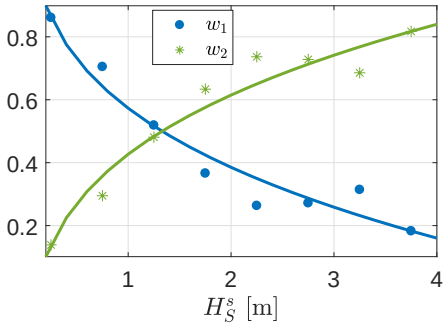

Figure 14: Weighting parameters for 2-folded von Mises mixture distribution of swell direction with fitting functions

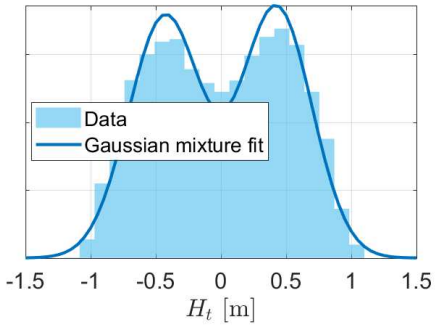

Figure 15: Tidal elevation

4. Simulation results

With an environmental model that contains a large number of variables where many of them are uncorrelated, numerical integration over the complete domain in combination with response calculation of offshore structures may become computationally too demanding and impractical to perform. Also, direct integration would not yield any error estimation. The efficiency of methods based on Monte Carlo simulation (MCS) does, however, not depend on the sampling domain. Latin Hypercube sampling (LHS) is another way of sampling from a high-dimensional domain and has proven efficient in terms of probability density estimation and in applications related to structural reliability analysis [31]. Hence, MCS or LHS with variance reduction techniques and various means of importance sampling related to the system dynamics are promising tools for use in probabilistic design where the stochastic variables are described by a joint probability model. See e.g. [32] and [33] for examples of application.

The obtained joint probability density function is tested against the pre-processed hindcast data by a Monte Carlo simulation. All 2D combinations in the data are compared with a root-mean-square-error (RMSE) estimate given as:

$$RMSE = \sqrt{\sum_j \sum_i (X_{ij} - Y_{ij})^2} \tag{9}$$

for fractions of empirical data X and simulated data Y in bin (i,j), an approach similar to [3]. Each data set is divided into the same 50 equally spaced intervals, so that $i, j = 1, \ldots, 50$. Results from 150 000 MCS are shown in Tab. 4. Except for the marginal swell directional distribution, the RMSE values are in general low, indicating good representation of both marginals on the diagonal and joint distributions elsewhere.

The resulting marginals are presented in the form of histograms to illustrate the similarities between the pre-processed hindcast data and simulated data. The wind speed and wind direction show a very good fit in Fig. 16. In Fig. 17, the wind sea parameters are compared, showing only a slight deviation for small values of the significant wave height and peak period. Swell sea and tidal elevation are presented in Fig. 18, and again the agreement is good, although the directional hindcast data is not completely described by a 2-fold von Mises distribution due to some irregularities.

Table 4: RMSE from simulations

	V	Θ_v	H_S^w	T_P^w	Θ_w^r	H_S^s	T_P^s	Θ_s	H_t
V	0.012	0.006	0.018	0.021	0.013	0.012	0.022	0.044	-
Θ_v	-	0.013	0.007	0.009	0.029	0.014	0.009	0.047	-
H_S^w	-	-	0.027	0.036	0.015	0.014	0.042	0.054	-
T_P^w	-	-	-	0.029	0.013	0.013	0.045	0.046	-
Θ_w^r	-	-	-	-	0.011	0.015	0.016	0.064	-
H_S^s	-	-	-	-	-	0.036	0.019	0.054	-
T_P^s	-	-	-	-	-	-	0.025	0.051	-
Θ_s	-	-	-	-	-	-	-	0.191	-
H_t	-	-	-	-	-	-	-	-	0.029

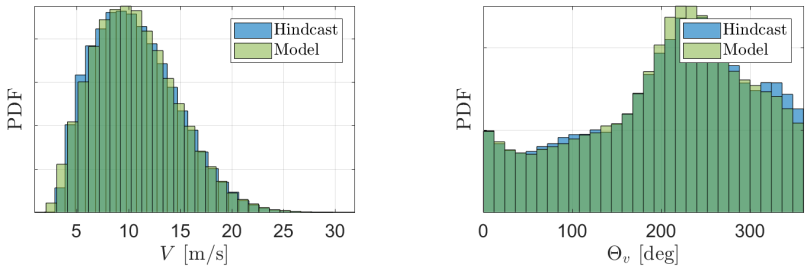

Figure 16: Pre-prcessed wind data compared to results from MCS

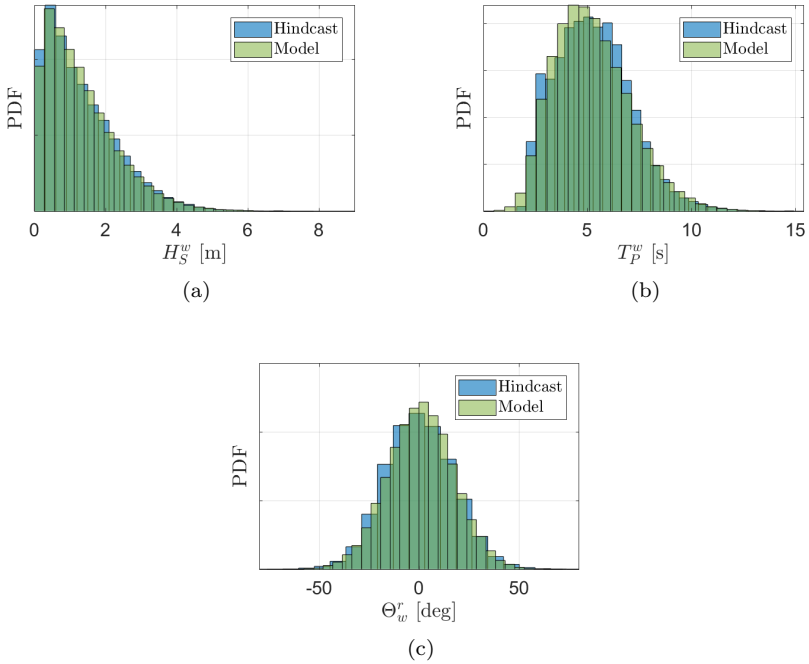

Figure 17: Pre-prcessed wind sea data compared to results from MCS

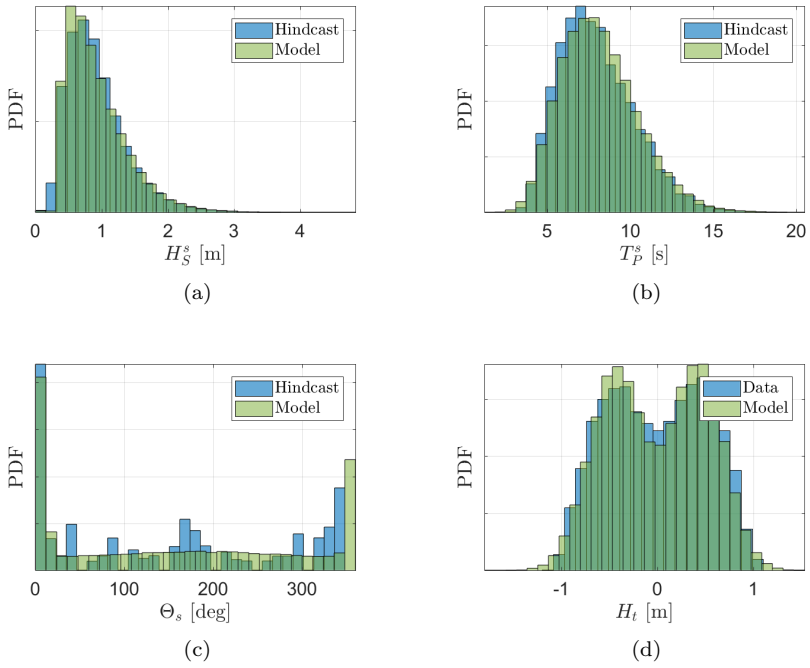

Figure 18: Pre-prcessed swell and tidal data compared to results from MCS

4.1. Environmental contours

To further compare the fitted model with the hindcast data, several environmental contours calculated using IFORM [1] have been established. The results are shown in Fig. 19a for 2D contours for wind speed and wind sea significant wave height and for peak period in Fig. 19b. From Fig. 19a, it can be observed that the model will allow slightly higher extreme wave heights for approximately $8 < V < 18$ than the hindcast data suggests. This is partly a result of the statistical uncertainty when fitting a distribution to hindcast data as higher classes of wave heights given wind speed include less observations. To investigate the assumption of independent wind sea and swell, the corresponding wave heights and contour lines are plotted in Fig. 19c. Overall, the hindcast data seems to lie inside the contour lines, without excessive out-crossings of the 50-year contour line. To illustrate some 3D effects, the significant wave height and peak period for wind sea is plotted in Fig. 19d for $22 < V < 24$. This domain contains very few data points and are subject to statistical uncertainty due to limited numbers of observations. Therefore, larger variations are observed in the peak period for a given wave height when extrapolating to 10 and 50 year return periods.

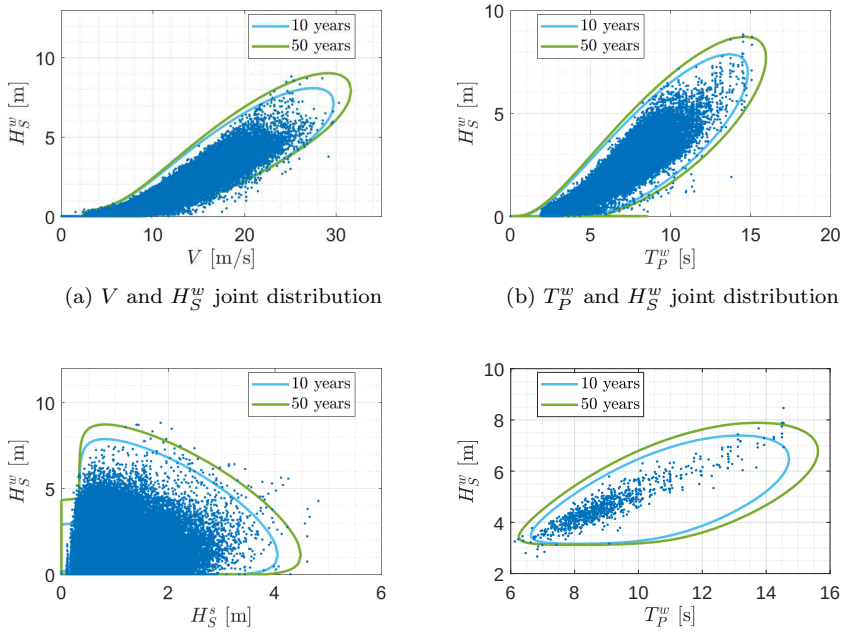

(a) V and H_S^w joint distribution

(b) T_P^w and H_S^w joint distribution

(c) H_S^s and H_S^w joint distribution

(d) T_P^w and H_S^w joint distribution for $22 < V < 24$m/s

Figure 19: Contour lines for environmental conmbinations with 10 and 50 year return periods including pre-processed hindcast data

5. Conclusion

A method for obtaining an analytic probabilistic description of the environmental parameters including directional effects is proposed and verified by hindcast data from a specific location in the North Sea. The model provides a good representation of the wind, wind sea and swell environment at the considered location. The model is meant to be used for calculations of environmental loads of marine structures, e.g. offshore wind turbines, in probabilistic design. A paper demonstrating its application will follow. A conservative description of the peak period for a given significant wave height is also demonstrated by use of the contour plots, which is a good tool for design of dynamically sensitive offshore structures subjected to higher order loading, like bottom-fixed monopile-mounted wind turbines [34].

A von Mises mixture distribution conditioned on the wind speed is successfully adopted for modelling the wind direction, and has proven very flexible for multi-directional processes. As a first approach, only conditioning the weights of the main wind directions in the folded von Mises distribution has proven very effective. The continuous directional distribution of wind speed which is

proposed can be used in probabilistic analysis of rotationally symmetric structures or as a response parameter for non-symmetric structures. To the authors' knowledge, a 3-parameter Weibull distribution of significant wave height conditioned on the wind speed has been established for the first time, and an efficient fitting method is presented in order to obtain a satisfactory fit. Also, a separate joint distribution for swell is useful especially for fatigue design and will allow to capture important response for structures sensitive to environmental directions, such as offshore wind turbines. In a similar manner, a description of the current velocity and direction may be included in the proposed joint model if such data exists.

Acknowledgement

This work has been carried out at the Centre for Autonomous Marine Operations and Systems (NTNU AMOS). The Norwegian Research Council is acknowledged as the main sponsor of NTNU AMOS. This work was supported by the Research Council of Norway through the Centres of Excellence funding scheme, Project number 223254 - NTNU AMOS. The authors would like to thank the Norwegian Meteorological Institute for providing hindcast data.

References

[1] S. Haver, S. R. Winterstein, Environmental contour lines: A method for estimating long term extremes by a short term analysis, Transactions - Society of Naval Architects and Marine Engineers 116 (2009) 116–127.

[2] E. M. Bitner-Gregersen, Joint Met-ocean Description for Design and Operations of Marine Structures, Applied Ocean Research 51 (2015) 279–292. doi:10.1016/j.apor.2015.01.007.

[3] E. Vanem, Copula-based Bivariate Modelling of Significant Wave Height and Wave Period and the Effects of Climate Change on the Joint Distribution, in: Proceedings of the 35th International Conference on Ocean, Offshore and Arctic Engineering, ASME, Busan, South Korea, 2016, pp. 1–12.

[4] E. Vanem, Joint statistical models for significant wave height and wave period in a changing climate, Marine Structures 49 (2016) 180–205. doi:10.1016/j.marstruc.2016.06.001.

[5] Y. Zhang, M. Beer, S. T. Quek, Long-term performance assessment and design of offshore structures, Computers & Structures 154 (2015) 101–115. doi:10.1016/j.compstruc.2015.02.029.

[6] E. M. Bitner-Gregersen, S. Haver, R. Løseth, Ultimate Limit States with Combined Load Processes, in: Proceedings of the 2nd Offshore and Polar Engineering Conference, 1992.

[7] J. Heideman, O. Hagen, C. Cooper, F.-E. Dahl, Joint Probability of Extreme Waves and Currents on Norwegian Shelf, Journal of Waterway, Port, Coastal, and Ocean Engineering 115 (4) (1989) 534–546.

[8] E. M. Bitner-Gregersen, S. Haver, Joint Environmental Model for Reliability Calculations, in: Proceedings of the First International Offshore and Polar Engineering Conference, 1991.

[9] DNV GL, RP-C205 Environmental conditions and environmental loads, Tech. rep. (2017).

[10] K. Johannessen, T. S. Meling, S. Haver, Joint Distribution for Wind and Waves in the Northern North Sea, International Journal of Offshore and Polar Engineering 12 (1) (2002) 1–8.

[11] L. Li, Z. Gao, T. Moan, Joint Environmental Data at Five European Offshore Sites for Design of Combined Wind and Wave Energy Devices, Journal of Offshore Mechanics and Arctic Engineering 137 (June) (2015) 1–16.

[12] E. M. Bitner-Gregersen, Distribution of Multidirectional Environmental Effects, in: Proceedings of the 15th International Conference on Ocean, Offshore and Arctic Engineering, ASME, Florence, Italy, 1996.

[13] E. M. Bitner-Gregersen, Joint Probabilistic Description for Combined Seas, in: Proceedings of the 24th International Conference on Offshore Mechanics and Arctic Engineering, 2005. doi:10.1115/OMAE2005-67382.

[14] G. Z. Forristall, On the Use of Directional Wave Criteria, Journal of Waterway, Port, Coastal, and Ocean Engineering 130 (6) (2004) 312–321.

[15] E. E. Bachynski, M. I. Kvittem, C. Luan, T. Moan, Wind-Wave Misalignment Effects on Floating Wind Turbines: Motions and Tower Load Effects, Journal of Offshore Mechanics and Arctic Engineering 136 (4) (2014) 41902.

[16] L. Barj, S. Stewart, G. Stewart, M. Lackner, J. Jonkman, A. Robertson, D. Matha, Wind/wave misalignment in the loads analysis of a floating offshore wind turbine, in: 32nd ASME Wind Energy Symposium, 2014. doi:10.2514/6.2014-0363.

[17] J.-T. Horn, J. R. Krokstad, J. Amdahl, Long-Term Fatigue Damage Sensitivity to Wave Directionality in Extra Large Monopile Foundations, Journal of Engineering for the Maritime Environmentdoi:10.1177/1475090217727136.

[18] J. Vega, Modeling Long Term Distribution of Mean Wave Direction, in: Proceedings of the 12th International Congress of the International Maritime Association of the Mediterranean, 2007, pp. 839–846.

[19] J. Mathisen, K. O. Ronold, G. Sigurdsson, Probabilistic Modelling for Reliability Analysis of Jackets, in: Proceedings of the 23rd International Conference on Offshore Mechanics and Arctic Engineering, ASME, 2004, pp. 231–239. doi:10.1115/OMAE2004-51227.

[20] J.-T. Horn, J. R. Krokstad, J. Amdahl, Joint Probability Distribution of Environmental Conditions for Design of Offshore Wind Turbines, in: Proceedings of the 36th International Conference on Ocean, Offshore and Arctic Engineering, Trondheim, Norway, 2017.

[21] N. Masseran, A. M. Razali, K. Ibrahim, M. T. Latif, Fitting a mixture of von Mises distributions in order to model data on wind direction in Peninsular Malaysia, Energy Conversion and Management 72 (2013) 94–102. doi:10.1016/j.enconman.2012.11.025.

[22] J. A. Carta, C. Bueno, P. Ramírez, Statistical modelling of directional wind speeds using mixtures of von Mises distributions: Case study, Energy Conversion and Management 49 (5) (2008) 897–907.

[23] M. Abramowitz, I. A. Stegun, Handbook of Mathematical Functions, 1965.

[24] C. Forbes, M. Evans, N. Hastings, B. Peacock, von Mises Distribution, in: Statistical Distributions, John Wiley & Sons, Inc., 2010, pp. 191–192. doi:10.1002/9780470627242.ch45.

[25] J. A. Carta, P. Ramírez, C. Bueno, A joint probability density function of wind speed and direction for wind energy analysis, Energy Conversion and Management 49 (6) (2008) 1309–1320. doi:10.1016/j.enconman.2008.01.010.

[26] M. Reistad, Ø. Breivik, H. Haakenstad, O. J. Aarnes, B. R. Furevik, J. R. Bidlot, A high-resolution hindcast of wind and waves for the North Sea, the Norwegian Sea, and the Barents Sea, Journal of Geophysical Research: Oceans 116 (5) (2011) 1–18. doi:10.1029/2010JC006402.

[27] DNV GL, Loads and site conditions for wind turbines, Tech. Rep. November (2016).

[28] A. Naess, O. Karpa, Statistics of bivariate extreme wind speeds by the ACER method, Journal of Wind Engineering and Industrial Aerodynamics 139 (2015) 82–88. doi:10.1016/j.jweia.2015.01.011.

[29] A. Semedo, R. Vettor, Ø. Breivik, A. Sterl, M. Reistad, C. G. Soares, D. Lima, The wind sea and swell waves climate in the Nordic seas, Ocean Dynamics 65 (2) (2015) 223–240. doi:10.1007/s10236-014-0788-4.

[30] R. L. Smith, J. C. Naylor, A Comparison of Maximum Likelihood and Bayesian Estimators for the Three- Parameter Weibull Distribution, Journal of the Royal Statistical Society. Series C (Applied Statistics) 36 (3) (1987) 358–369.

[31] A. Olsson, G. Sandberg, O. Dahlblom, On Latin hypercube sampling for structural reliability analysis, Structural Safety 25 (1) (2003) 47–68. doi:10.1016/S0167-4730(02)00039-5.

[32] Y. M. Low, A variance reduction technique for long-term fatigue analysis of offshore structures using Monte Carlo simulation, Engineering Structures 128 (2016) 283–295. doi:10.1016/j.engstruct.2016.09.047.

[33] Y. Gao, Y. M. Low, An efficient importance sampling method for long-term fatigue assessment of deepwater risers with time domain analysis, Probabilistic Engineering Mechanics 45 (2016) 102–114. doi:10.1016/j.probengmech.2016.04.003.

[34] J. Krokstad, C. Stansberg, A. Nestegaard, T. Marthinsen, A New Non-slender Ringing Load Approach Verified Against Experiments, Journal of Offshore Mechanics and Arctic Engineering 120 (1) (1998) 20–29. doi:10.1115/1.2829515.

Appendix

Table 5: Fitting constants

Var.	Par.	Arg.	Marg.	p_1	p_2	p_3	p_4	p_5	p_6	p_7
V	α	-	9.49e+00	9.49e+00	0	1	0	1	0	1
	β	-	2.19e+00	2.19e+00	0	1	0	1	0	1
	γ	-	2.28e+00	2.28e+00	0	1	0	1	0	1
Θ_v	w_1	v	2.77e-01	0	0	1	4.28e-01	-1.06e-03	1	2.52e+00
	w_2	v	4.33e-01	0	0	1	1	-1.62e+03	1.89e+01	-2.28e+00
	w_3	v	2.90e-01	0	0	1	2.26e+00	-1.63e+00	5.88e+00	1.03e-01
	μ_1	-	1.11e+02	1.11e+02	0	1	0	1	0	1
	μ_2	-	2.27e+02	2.27e+02	0	1	0	1	0	1
	μ_3	-	3.24e+02	3.24e+02	0	1	0	1	0	1
	κ_1	-	1.02e+00	1.02e+00	0	1	0	1	0	1
	κ_2	-	2.02e+00	2.02e+00	0	1	0	1	0	1
	κ_3	-	1.73e+00	1.73e+00	0	1	0	1	0	1
H_S^w	α	v	1.56e+00	7.04e-01	0	0	1.32e+00	-1.23e+02	0	-2.00e+00
	β	v	1.43e+00	1.51e+00	4.41e+01	-1.39e+00	0	1	0	1
	γ	v	-9.39e-02	-5.94e-01	6.96e-03	2.00e+00	0	1	0	1
T_P^w	μ	h	1.61e+00	0	1.58e+00	2.45e-01	0	1	0	1
	σ	h	3.54e-01	0	1.35e-01	-2.14e-01	0	1	0	1
Θ_w^r	μ	h	2.38e-01	4.45e+00	-2.57e+00	1	0	1	0	1
	σ	h	1.71e+01	1.63e+01	0	1	0	1	0	1
H_S^s	α	-	6.38e-01	6.38e-01	0	1	0	1	0	1
	β	-	1.32e+00	1.32e+00	0	1	0	1	0	1
	γ	-	3.32e-01	3.32e-01	0	1	0	1	0	1
T_P^s	μ	h_s	2.03e+00	0	2.11e+00	1.45e-01	0	1	0	1
	σ	h_s	2.81e-01	0	0	1	3.22e-01	-2.97e-01	0	1
Θ_s	w_1	h_s	6.93e-01	1.53e+00	-9.53e-01	2.60e-01	0	1	0	1
	w_2	h_s	3.07e-01	-5.26e-01	9.53e-01	2.60e-01	0	1	0	1
	μ_1	-	1.80e+02	1.80e+02	0	1	0	1	0	1
	μ_2	-	3.00e+00	3.00e+00	0	1	0	1	0	1
	κ_1	-	1.71e-01	1.71e-01	0	1	0	1	0	1
	κ_2	-	7.42e+01	7.42e+01	0	1	0	1	0	1
H_t	w_1	-	5.01e-01	5.01e-01	0	1	0	1	0	1
	w_2	-	4.99e-01	4.99e-01	0	1	0	1	0	1
	μ_1	-	4.27e-01	4.27e-01	0	1	0	1	0	1
	μ_2	-	-4.30e-01	-4.30e-01	0	1	0	1	0	1
	σ_1	-	7.35e-02	7.35e-02	0	1	0	1	0	1
	σ_2	-	7.79e-02	7.79e-02	0	1	0	1	0	1